Zirconia-Supported MoO_x Catalysts for the Selective Oxidation of Dimethyl Ether to Formaldehyde: Structure, Redox Properties, and Reaction Pathways

Haichao Liu, Patricia Cheung, and Enrique Iglesia*

Department of Chemical Engineering, University of California at Berkeley, Berkeley, California 94720

Received: October 1, 2002; In Final Form: January 31, 2003

Dimethyl ether (DME) reacts to form formaldehyde with high selectivity at 500−600 K on MoO_x−ZrO_2 catalysts with a wide range of MoO_x surface density (0.5−50.1 Mo/nm^2) and local structure (monomers, oligomers, MoO_3 crystallites, and $ZrMo_2O_8$). Reaction rates (per Mo-atom) increased markedly as MoO_x surface density increased from 2.2 to 6.4 Mo/nm^2 and two-dimensional polymolybdates and MoO_3 clusters became the prevalent active species. The rate of incipient stoichiometric reduction of MoO_x−ZrO_2 samples in H_2 also increased with increasing MoO_x surface density, suggesting that catalytic turnovers involve redox cycles that become faster as the size and dimensionality of MoO_x domains increase. DME reaction rates (per Mo-atom) decreased as MoO_x surface densities increased above 6.4 Mo/nm^2, as MoO_3 and $ZrMo_2O_8$ clusters with increasingly inaccessible MoO_x species form. On MoO_x and $ZrMo_2O_8$, areal reaction rates reach a constant value at MoO_x surface densities above 10 Mo/nm^2, as the exposed surfaces become covered with the respective active species. $ZrMo_2O_8$ surfaces were more reducible in H_2 than MoO_x surfaces and showed higher areal reaction rates. Reaction rates were nearly independent of O_2 pressure, but the reaction order in DME decreased from one at low pressures (<40 kPa) to zero at higher pressures (>60 kPa). DME reacts via primary pathways leading to HCHO, methyl formate, and CO_x, with rate constants k_1, k_2, and k_3, respectively, and via secondary HCHO conversion to methylformate (k_4) and CO_x (k_5). Primary HCHO selectivities (and $k_1/(k_2 + k_3)$ ratios) increased with increasing MoO_x surface density on MoO_x-containing samples and reached values of 80−90% above 10 Mo/nm^2. Kinetic ratios relevant to secondary HCHO reactions ($k_1/[(k_4 + k_5)C_{Ao}]$; C_{Ao} inlet DME concentration) also increased with increasing MoO_x surface density to values of ∼0.1 and 0.8 on MoO_x and $ZrMo_2O_8$ structures (at the constant inlet DME concentration C_{Ao}), respectively. Thus, increasing the coverage of ZrO_2 surfaces with MoO_x or $ZrMo_2O_8$ leads to more selective structures for HCHO synthesis from DME.

1. Introduction

Many recent studies have addressed the conversion of methane to chemicals and transportation fuels.[1−6] An attractive route to chemicals involves the selective conversion of methane to formaldehyde[2,7−12] and the subsequent conversion of formaldehyde to larger molecules containing C−C bonds. Formaldehyde (HCHO) synthesis via direct oxidation of methane with O_2 leads to low yields, because of fast sequential HCHO decomposition and combustion reactions. Most previous studies have reported HCHO yields below 5%,[7−10] but HCHO yields as high as ∼18% have been recently reported.[5,11,12] As a result, indirect routes for methane conversion to chemicals and liquid fuels are industrially practiced; for example, formaldehyde is produced via the synthesis of methanol from synthesis gas (H_2/CO) and its subsequent oxidative dehydrogenation to HCHO. Here, we report an alternate route to HCHO via the selective oxidation of dimethyl ether (DME) produced from H_2/CO mixtures.

Fe−Mo oxides and Ag-based catalysts[13,14] are currently used for methanol oxidation to HCHO. The pathways and catalyst requirements for this reaction have been widely studied.[14,15] Lattice oxygen atoms are used in rate-limiting steps involving hydrogen abstraction from adsorbed methoxide species ($CH_3O^{-\delta}$). These methoxide species can also be formed via cleavage of weak C−O bonds in DME (CH_3OCH_3),[16,17] but previous reports consist of only a few patents.[18−22] The limited scope of these previous reports reflects the historically higher cost of DME relative to methanol; direct synthesis gas routes to DME, however, have been recently developed and they provide more favorable thermodynamics and economics than methanol synthesis.[23−25] A potential DME distribution infrastructure in some developing countries and the benign properties of DME as a fuel[24,25] also render it attractive as an alternate intermediate for the synthesis of chemicals currently produced from methanol.

These considerations led us to examine the catalytic chemistry of DME and specifically its oxidative conversion to HCHO on supported metal oxides. Well-dispersed domains of metal oxides, predominately present as two-dimensional structures, provide an effective balance between reactivity and accessibility of oxide surfaces. Our preliminary studies identified MoO_x and VO_x as the preferred active oxides.[26] MoO_x domains supported on Al_2O_3, ZrO_2, or SnO_2 showed high primary HCHO selectivities (80−98%).[26,27] HCHO formation rates on these catalysts were significantly higher than previously reported,[18−22] even at temperatures much lower than in these earlier studies.

Here, we describe a detailed study of the reducibility, structure, and catalytic properties of ZrO_2-supported MoO_x samples with a wide range of MoO_x densities; surface densities were varied by changing the Mo content and the thermal treatment conditions. These samples consist of MoO_x domains of varying size and dimensionality or of surface layers of

* Author to whom correspondence should be addressed. Tel: (510) 642-9673. Fax: (510) 642-4778. E-mail: iglesia@cchem.berkeley.edu.

10.1021/jp0221744 CCC: $25.00
Published on Web 04/04/2003

TABLE 1: Surface Areas and MoO_x Surface Density for MoO_x/ZrO_2 Catalysts Treated at 723, 773, and 873 K

	723 K			773 K		873 K	
sample	MoO_3 content (wt %)	surface area (m^2/g)	MoO_x surface density (Mo/nm^2)	surface area (m^2/g)	MoO_x surface density (Mo/nm^2)	surface area (m^2/g)	MoO_x surface density (Mo/nm^2)
$1MoO_x/ZrO_2$	1.0%	118.8	0.3	105.6	0.4	85.6	0.5
$6MoO_x/ZrO_2$	5.7%	130.0	1.8	110.3	2.2	97.1	2.5
$11MoO_x/ZrO_2$	11.0%	145.9	3.2	132.6	3.5	103.4	4.5
$21MoO_x/ZrO_2$	20.7%	153.7	5.6	136.3	6.4	102.7	8.4
$29MoO_x/ZrO_2$	29.3%	114.0	10.7	96.9	12.6	64.6	20.0
$37MoO_x/ZrO_2$	37.0%	99.6	15.5	73.9	20.9	49.3	31.4
$44MoO_x/ZrO_2$	44.0%	83.5	22.0	60.2	30.6	36.7	50.1

MoO_x-ZrO_2 mixed oxides, depending on the thermal treatment and the MoO_x surface density. This study addresses the structural and site requirements for primary and secondary pathways relevant to DME oxidation reactions. It also explores the redox nature of the catalytic sequence involved in HCHO synthesis and the fundamental relationships among the size, structure, and reducibility of MoO_x domains and their catalytic reactivity.

2. Experimental Section

2.1. Synthesis of Catalytic Materials. MoO_x/ZrO_2 was prepared by incipient wetness impregnation of precipitated $ZrO(OH)_2$ with aqueous $(NH_4)_2Mo_2O_8$ solutions (99%, Aldrich).[28,29] $ZrO(OH)_2$ was prepared via precipitation of zirconyl chloride solutions (98%, Aldrich) at a pH of 10, maintained constant by continuous addition of NH_4OH (29.8%, Fisher Scientific). The precipitated solids were washed with a NH_4OH solution of pH ~8 until Cl ions were no longer detected by $AgNO_3$ in the filtrate and then dried overnight in ambient air at 393 K. The impregnated solids were also dried overnight in ambient air at 393 K and then treated in flowing dry air at 723, 773, or 873 K for 3 h. The Mo content was set by the Mo concentration in the impregnating solution.

These MoO_x/ZrO_2 samples were characterized using X-ray diffraction (XRD) and UV−visible, Raman, X-ray absorption near-edge (XANES), and fine structure (XAFS) spectroscopies.[28,29] BET surface areas were measured using N_2 at its normal boiling point. MoO_x surface densities are reported as Mo/nm^2 using the measured Mo contents and BET surface areas. Table 1 shows a summary of the Mo contents, BET surface areas, and surface densities for the samples used in this study.

2.2. Stoichiometric Reduction of MoO_x/ZrO_2 in H_2. Reduction rates of MoO_x/ZrO_2 were measured using H_2 as the reductant and a Quantasorb surface area analyzer (Quantachrome Corporation) modified with electronic mass flow controllers. MoO_x/ZrO_2 samples (10 mg Mo) were placed in a quartz cell (4 mm-i.d.) containing a quartz thermowell in contact with the samples. The temperature was increased linearly from 298 to 1253 K at 0.167 K s^{-1} in flowing 20% H_2/Ar (1.33 cm^3s^{-1}) (Matheson UHP). The H_2 content in the effluent was measured by thermal conductivity after the H_2O formed during reduction was removed from the effluent stream using a 13X molecular sieve trap held at ambient temperature. The conductivity detector response was calibrated from the complete reduction of CuO powders (99.995%, Aldrich). Reduction rate constants were obtained from the initial rates of H_2 consumption using previously reported kinetic analysis protocols.[30,31]

2.3. Dimethyl Ether Catalytic Oxidation Rates and Selectivities. Dimethyl ether reaction rates and selectivities were measured in a fixed-bed quartz microreactor using MoO_x/ZrO_2 samples (0.3 g) diluted with quartz powder (1.0 g) in order to avoid temperature gradients within the catalyst bed. Samples were treated in flowing 20% O_2/He (0.67 cm^3 s^{-1}) for 1.5 h at 723, 773, or 873 K before catalytic measurements. Catalytic rates and selectivities were measured at 453−553 K, typically using a mixture of DME (80 kPa; 99.5%, Praxair), O_2 (18 kPa), and N_2 (2 kPa) (Praxair, certified O_2/N_2 mixture). For kinetic measurements, DME, O_2, and H_2O partial pressures in the reactant stream were varied in the ranges 5−80 kPa, 5−40 kPa, and 0−15 kPa, respectively. Homogeneous DME reactions were detected only above 593 K in empty reactors. Water was added to DME/O_2 reactant mixtures by passing a controlled flow of 20% H_2/He over a bed of CuO/Al_2O_3 (13 wt %, Aldrich) held at 623 K in order to combust all the H_2 to H_2O using the lattice oxygen atoms in CuO. All transfer lines after the introduction of H_2O were kept above 393 K in order to prevent condensation.

The reactor effluent was analyzed by on-line gas chromatography (Hewlett-Packard 6890 GC) using a methyl silicone capillary column (HP-1, 30 m × 0.25 mm × 0.25 μm film thickness) connected to a flame ionization detector and a Porapak Q packed column (80−100 mesh, 1.82 m × 3.18 mm) connected to a thermal conductivity detector. Methanol, formaldehyde (HCHO), methylformate (MF), CO, CO_2, H_2O, and traces of dimethoxymethane (DMM) were the only products detected. Detailed HCHO calibrations were carried out in order to ensure that neither decomposition nor oligomerization of HCHO occurred in the transfer lines, the on-line sampling valve, or the chromatograph injector or column.

Reaction rates and product selectivities were measured as a function of DME conversion, which was varied through changes in reactant flow rate between 1.5 and 10 cm^3 (STP)/g s^{-1}. DME conversion levels were kept below 10% and DME reaction rates and selectivities were extrapolated to zero residence time in order to obtain primary reaction rates and selectivities. DME reaction rates and selectivities are reported in two ways. One method considers CH_3OH as a reaction product, while the other lumps any CH_3OH formed with unreacted DME and considers selectivities on a CH_3OH-free basis. The latter approach seems appropriate in view of the available pathways for DME−CH_3OH interconversion and for CH_3OH conversion to HCHO. All selectivities are reported on a carbon basis as the percentage of the carbon atoms in the reacted DME appearing as each product.

3. Results

3.1. Effects of Reactant Residence Time. DME conversion rates are shown in Figure 1 as a function of reactant residence time at 513 K on 20.7% MoO_x/ZrO_2 ($21MoO_x/ZrO_2$ in Table 1) (treated in air at 773 K; 6.4 Mo/nm^2 surface density). The ZrO_2 support in this sample is predominately covered by two-dimensional polymolybdate species.[28,29] DME conversion rates decreased slightly with increasing residence time as a result of the weak H_2O inhibition effects discussed below. The primary DME reaction rate was 12.2 mol/g-atom Mo-h. CH_3OH, HCHO, methylformate (MF), dimethoxymethane (DMM), and CO_x (CO + CO_2) were detected in the reactor effluent. The selectivity for the predominant HCHO product decreased with increasing residence time and DME conversion (Figure 1), while methyl-

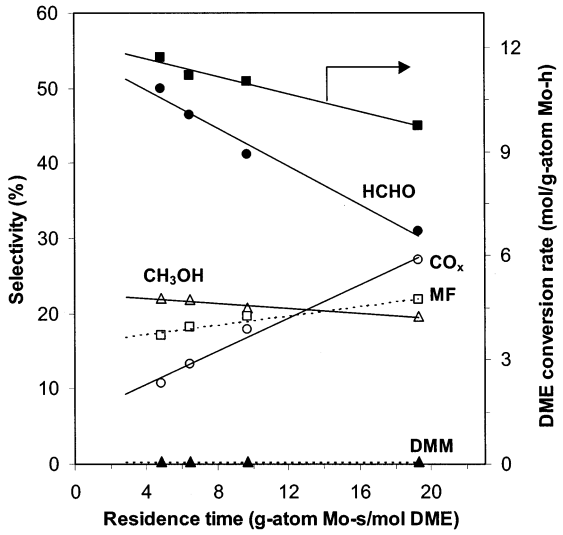

Figure 1. DME reaction rates and selectivities as a function of reactant residence time at 513 K on $21MoO_x/ZrO_2$ (6.4 Mo/nm^2) treated at 773 K (80 kPa CH_3OCH_3, 18 kPa O_2, 2 kPa N_2).

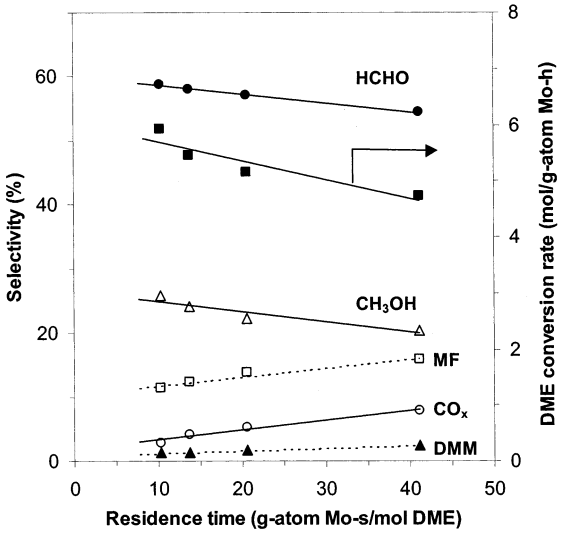

Figure 2. DME reaction rates and selectivities as a function of reactant residence time at 513 K on $44MoO_x/ZrO_2$ (50.1 Mo/nm^2) treated at 873 K (80 kPa CH_3OCH_3, 18 kPa O_2, 2 kPa N_2).

formate, dimethoxymethane, and CO_x selectivities concurrently increased. The selectivity to CH_3OH was essentially independent of residence time. The primary selectivities to CH_3OH (23.0%), HCHO (57.1%), MF (15.5%), DMM (0.3%), and CO_x (4.1%) were all nonzero, indicating that these products can be formed directly from DME.

Figure 2 shows the effects of residence time on DME conversion rates and selectivities at 513 K on $44MoO_x/ZrO_2$ treated at 873 K (50.1 Mo/nm^2). This sample consists predominately of $ZrMo_2O_8$ and ZrO_2.[28,29] The primary products and the effects of residence time on DME conversion rates were similar to those observed on $21Mo/ZrO_2$ (6.4 Mo/nm^2; Figure 1), which contains predominately two-dimensional polymolybdate structures. The effects of residence time on HCHO selectivities were much weaker on $44Mo/ZrO_2$ (50.1 Mo/nm^2) than on $21Mo/ZrO_2$ (6.4 Mo/nm^2). Thus, it appears that $ZrMo_2O_8$ structures catalyze secondary HCHO reactions less effectively than the polymolybdate domains prevalent in $21Mo/ZrO_2$ (6.4 Mo/nm^2) (cf. Figures 1 and 2).

CH_3OH selectivities remained almost constant with changes in residence time on all catalysts. CH_3OH appears to form in a parallel path, possibly involving hydrogen transfer among the methoxide species also involved in HCHO formation. In view of these parallel pathways and of the catalytic routes available for the concurrent dehydration and oxidative dehydrogenation of CH_3OH, we consider CH_3OH products as part of the DME reactant pool and we report hereinafter rates and selectivities on a CH_3OH-free basis.

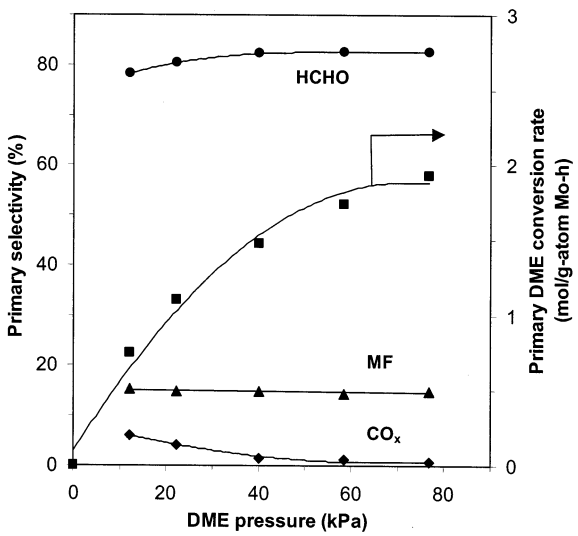

Figure 3. Effect of DME partial pressure on primary DME reaction rates and selectivities to HCHO, MF, and CO_x at 493 K on $44MoO_x/ZrO_2$ (50.1 Mo/nm^2) treated at 873 K (9 kPa O_2, 1 kPa N_2, He balance).

3.2. Effects of CH_3OCH_3, O_2, and H_2O Concentrations on Reaction Rate and Selectivity. The effects of varying CH_3OCH_3, O_2, and H_2O partial pressures on DME conversion rates and selectivities were examined on several MoO_x/ZrO_2 (3.5, 6.4, 8.4, and 50.1 Mo/nm^2) samples with MoO_x or $ZrMo_2O_8$ structures. The observed kinetic responses were very similar on all samples. Here, we show detailed kinetic results only on $44MoO_x/ZrO_2$ (50.1 Mo/nm^2; treated at 873 K); this sample contains predominately $ZrMo_2O_8$.

Figure 3 shows primary DME conversion rates and primary selectivities to HCHO, MF, and CO_x at 493 K and 9 kPa O_2 as a function of DME partial pressure (10−80 kPa) without water in the reactant mixture. Primary DME conversion rates increased almost linearly with DME partial pressure from 10 to 40 kPa, and then more weakly at higher DME pressures, until reaction rates became nearly independent of DME pressure above 60 kPa. This behavior suggests surface saturation by one or more DME-derived reactive intermediates as DME pressure increases. Primary MF (14.8%) and DMM (1.0%) selectivities were almost independent of DME pressure, while primary CO_x selectivities decreased from 6.0% to a constant value of 1.5% as the DME pressure increased from 10 to 40 kPa. Concurrently, HCHO selectivities increased from 78.3 to 82.7% (Figure 3).

The effects of O_2 partial pressure were examined at DME pressures of 20 and 80 kPa (Figure 4a,b), which correspond to regimes in which DME reaction orders are near-first and -zero, respectively (see Figure 3). Primary DME conversion rates at 20 kPa DME were unaffected by O_2 partial pressure in the range 5−40 kPa (Figure 4a). An increase in O_2 pressure from 5 to 20 kPa at 80 kPa DME led to a slight increase in primary DME conversion rates (Figure 4b); thus, reaction rates are nearly independent of O_2 partial pressure throughout this DME concentration range. Primary selectivities were also essentially unaffected by O_2 partial pressure (Figure 4). The addition of water (15 kPa) to DME/O_2 reactant mixtures at levels higher

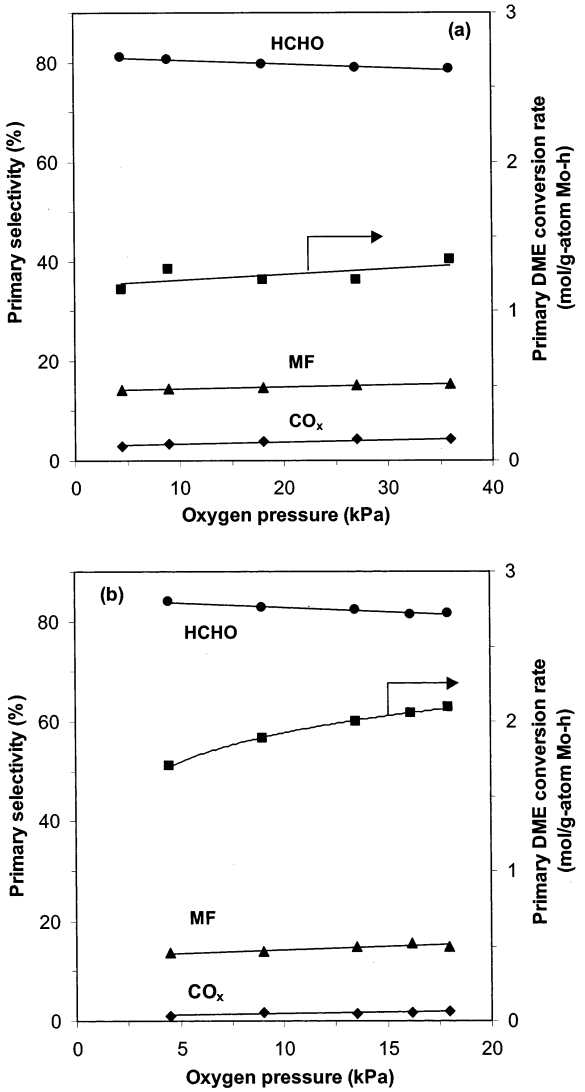

Figure 4. Effect of O_2 partial pressure on primary DME reaction rate and selectivities to HCHO, MF, and CO_x at 493 K at 20 kPa DME (a) and 80 kPa DME (b) (He balance, without added water) on $44MoO_x/ZrO_2$ (50.1 Mo/nm^2) treated at 873 K.

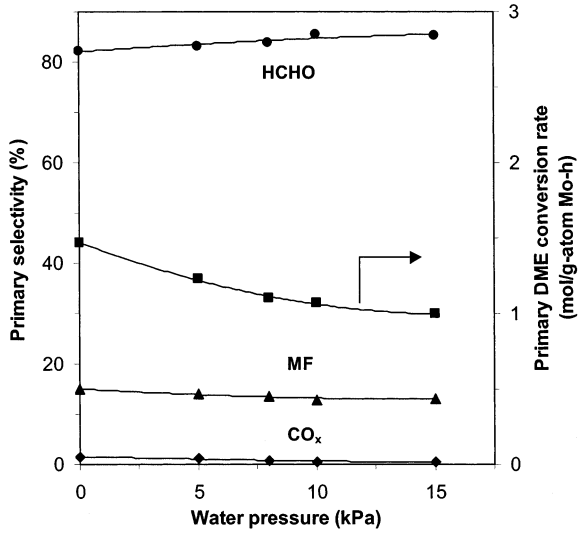

Figure 5. Effect of water partial pressure on primary DME reaction rate and selectivities to HCHO, MF, and CO_x at 493 K on $44MoO_x/ZrO_2$ (50.1 Mo/nm^2) treated at 873 K (40 kPa CH_3OCH_3, 9 kPa O_2, 1 kPa N_2, He balance).

than those prevalent during DME reactions led to a decrease in DME conversion rates (from 1.4 to 1.0 mol/g-atom Mo-h) without significant changes in primary selectivities (Figure 5). These water inhibition effects are consistent with the small decrease in DME conversion rates observed with increasing reactant residence time and DME conversion (Figures 1 and 2).

3.3. Effects of MoO_x Surface Density on DME Reaction Rate and Selectivity. The structure of the MoO_x domains present on MoO_x/ZrO_2 depends on MoO_x surface density and thermal treatment.[28,29] X-ray diffraction and UV−visible and Raman spectroscopic studies have shown that MoO_x/ZrO_2 samples contain two types of MoO_x structures. For surface densities above 5 Mo/nm^2 and thermal treatments at 873 K or higher temperatures, samples contain predominately $ZrMo_2O_8$ structures; similar treatments led to two-dimensional polymolybdates and MoO_3 crystallites (denoted as MoO_x structures) for samples with lower surface densities.[28,29] At all surface densities, MoO_x/ZrO_2 samples treated in air at 723 or 773 K contained predominately two-dimensional polymolybdates and MoO_3 crystallites.[28,29] The structural evolution of MoO_x domains from monomolybdates, to two-dimensional polymolybdates, and ultimately to three-dimensional MoO_3 crystallites was confirmed by the monotonic decrease in the UV−visible edge energy observed with increasing MoO_x surface density.[28]

Figure 6a shows the effects of MoO_x surface density and of the concurrent structural and compositional changes on primary DME reaction rates (per Mo-atom). On samples containing predominately MoO_x structures, these rates increased with increasing MoO_x surface density; they reached a maximum value at ∼6.4 Mo/nm^2, and then decreased at higher Mo surface densities. On $ZrMo_2O_8$ species, DME reaction rates decreased monotonically as the MoO_x surface density increased from 8.4 to 50.1 Mo/nm^2. At each (nominal) surface density, $ZrMo_2O_8$ samples showed higher rates (per Mo-atom) than MoO_x/ZrO_2 samples consisting of polymolybdate domains and MoO_x clusters. Treatment of $11MoO_x/ZrO_2$ at 873 K led to a 2-fold increase in DME reaction rates relative to those measured after treatment at 723 or 773 K (Figure 6a), even though Mo surface densities were essentially unchanged by this treatment (3.2−4.5 Mo/nm^2) (Table 1).

DME reaction rates normalized per (BET) total surface area are shown in Figure 6b for all samples. These rates increased monotonically with increasing MoO_x surface density and reached a constant value of 0.08 mmol/m^2-h at surface densities above 6.4 Mo/nm^2 for MoO_x species (two-dimensional polymolybdates or MoO_3 crystallites). These areal rates were unaffected by surface density on $ZrMo_2O_8$-containing samples (0.45 mmol/m^2-h), but they were significantly higher than on samples containing MoO_x species.

The effects of MoO_x surface density and local MoO_x structure on primary selectivities are shown in Figure 7a−c. On MoO_x-containing samples, primary HCHO selectivities increased with increasing MoO_x surface density and they reached a value of ∼90% for surface densities above 10 Mo/nm^2. HCHO selectivities on $ZrMo_2O_8$ species were slightly lower (∼80%); they were not influenced by MoO_x surface density (Figure 7a). Methylformate selectivities on MoO_x-containing samples decreased with increasing surface density to a constant value of ∼7% for surface densities above 10 Mo/nm^2. On $ZrMo_2O_8$ samples, methylformate selectivities were very similar (∼15%) at all Mo surface densities (8.4−50.1 Mo/nm^2) (Figure 7b). Primary CO_x selectivities decreased to ∼4% at Mo surface densities above 10 Mo/nm^2 on MoO_x samples; they were also ∼4%, but they

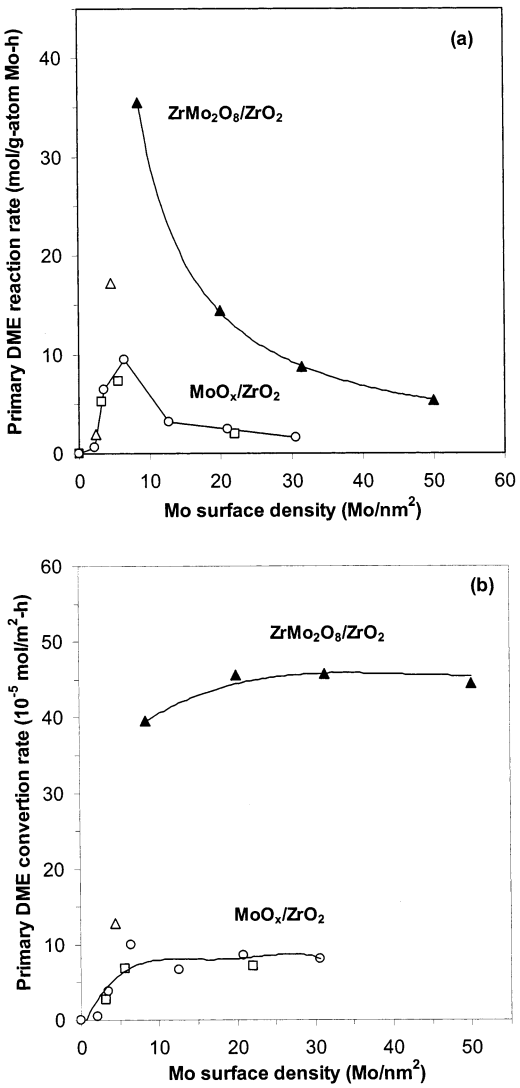

Figure 6. Dependence of primary DME reaction rates normalized per Mo atom (a) and per catalyst surface area (b) on MoO_x surface density for MoO_x/ZrO_2 catalysts (pretreated in air at 723 K (□), 773 K (○), and 873 K (△, ▲)) (513 K, 80 kPa CH_3OCH_3, 18 kPa O_2, 2 kPa N_2).

were not influenced by MoO_x surface density on $ZrMo_2O_8$ samples (Figure 7c).

Our recent transient and isotopic studies, taken together with the observed zero-order O_2 dependence of DME rates and selectivities (Figure 4a,b), suggest that DME reactions occur via a redox mechanism using lattice oxygen atoms at rates apparently limited by C−H bond cleavage in adsorbed methoxide (CH_3O*) intermediates.[32] C−H bond activation in CH_3O* species would involve the incipient reduction of MoO_x structures and the formation of low steady-state concentrations of reduced centers, which are continuously reoxidized by O_2 in order to complete a catalytic turnover. Therefore, the strong observed effects of MoO_x surface density and structure on DME reaction rates may reflect the ability of MoO_x domains to undergo local reduction during each catalytic turnover. This proposal is confirmed by measurements of the reducibility of MoO_x/ZrO_2 samples reported in the next section, which show a parallel increase in the rates of stoichiometric reduction in H_2 and of catalytic DME oxidation as MoO_x surface density increases.

3.4. Reduction Rates of MoO_x/ZrO_2 Samples in H_2. Reduction rates of MoO_x/ZrO_2 in H_2 were measured from the incipient rate of hydrogen consumption and oxygen removal as the sample temperature increased from 298 to 1253 K. The

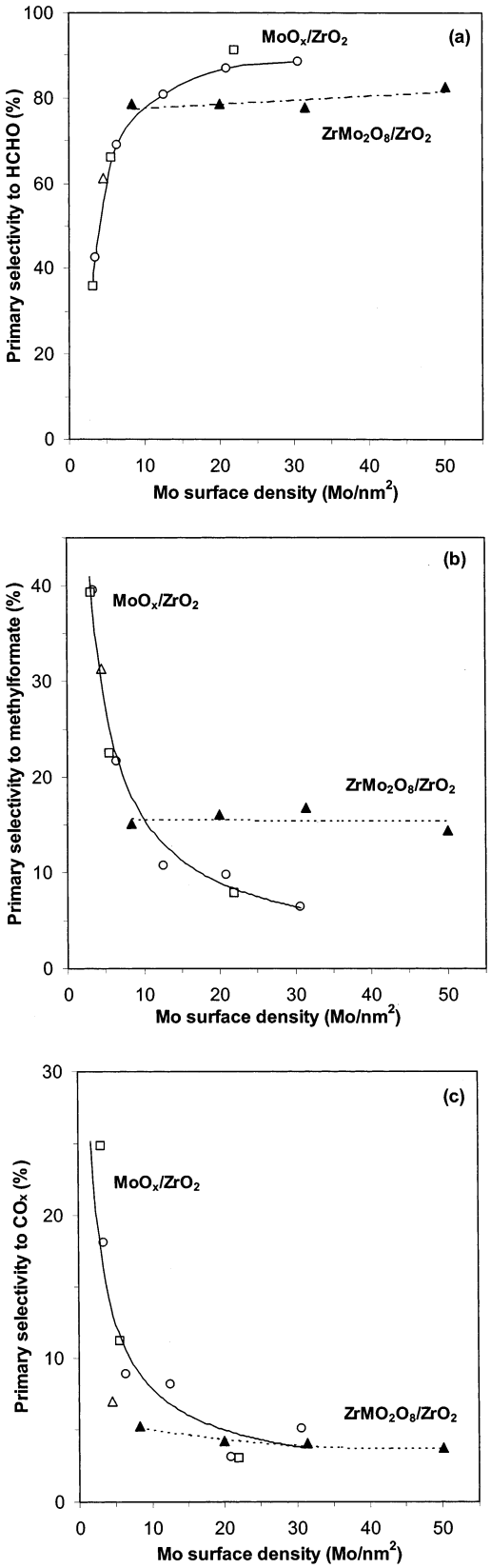

Figure 7. Dependence of primary selectivities to HCHO (a), MF (b), and CO_x (c) on MoO_x surface density for MoO_x/ZrO_2 catalysts (pretreated in air at 723 K (□), 773 K (○), and 873 K (△, ▲)) (513 K, 80 kPa CH_3OCH_3, 18 kPa O_2, 2 kPa N_2).

incipient reduction rates in H_2 for a given metal oxide reflect the removal of a few oxygen atoms, leading to surfaces with an extent of reduction similar to that prevalent during steady-state catalytic reactions involving redox cycles, such as the

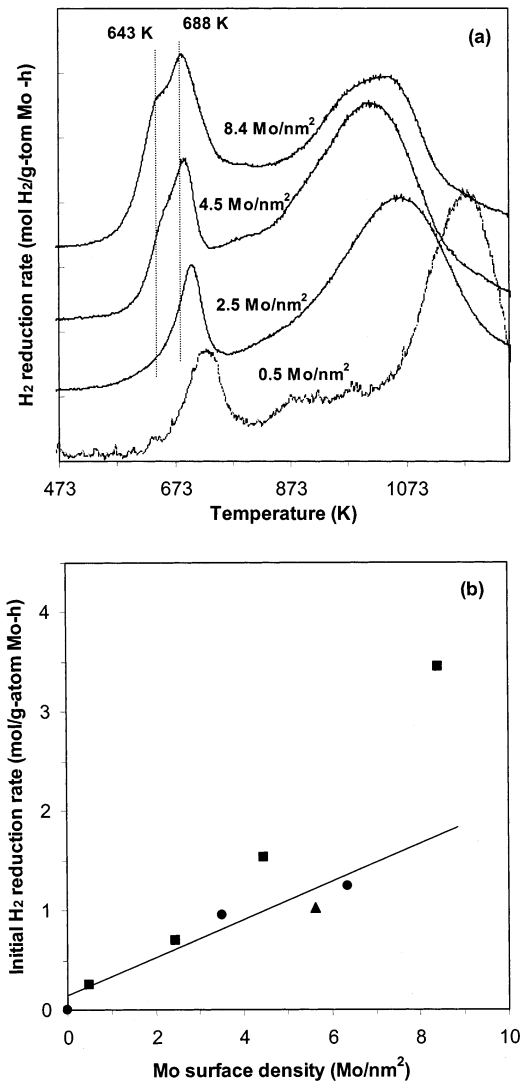

Figure 8. (a) Temperature-programmed reduction profiles for MoO_x/ZrO_2 catalysts treated at 873 K in air; (b) initial H_2 reduction rate at 623 K as a function of MoO_x surface density and MoO_x structure for MoO_x/ZrO_2 samples (pretreated in air at 723 K (▲), 773 K (●), and 873 K (■)).

oxidative dehydrogenation of alkanes.[31,33] The stoichiometric reduction of oxides with H_2 involves H_2 dissociation and the formation of surface OH groups similar in structure to those formed via H-abstraction from methoxy groups during HCHO synthesis from methanol or DME on oxide surfaces.

Figure 8a shows H_2 reduction rates for MoO_x/ZrO_2 samples treated in air at 873 K. Two reduction peaks are apparent and their relative intensities are consistent with the sequential reduction of Mo^{6+} to Mo^{4+} and of Mo^{4+} to Mo^0.[31,34,35] The low-temperature peak shifts from ~730 K to ~685 K as the MoO_x surface density increased from 0.5 to 8.4 Mo/nm^2. An additional shoulder appears at ~645 K for the sample with 8.4 Mo/nm^2 (Figure 8a), but the same $21MoO_x/ZrO_2$ sample treated at 723 K (5.6 Mo/nm^2) or 773 K (6.4 Mo/nm^2) lacks this feature. This feature corresponds to the reduction of Mo^{6+} to Mo^{4+} in Mo−O−Zr structures present in $ZrMo_2O_8$, which forms only after treatment at 873 K. These data suggest that the rates of Mo^{6+} to Mo^{4+} reduction steps are higher on larger MoO_x structures than on smaller ones; they are also higher on $ZrMo_2O_8$ domains than on polymolybdate structures.

In-situ X-ray absorption studies during reaction have shown that few reduced Mo^{4+} centers (<5%) are present during DME reactions at 513 K on these samples.[32] Thus, the very initial stages of Mo^{6+} to Mo^{4+} reduction steps are most relevant to the redox dynamics required in catalytic DME reactions. We have previously reported an analysis protocol for the kinetics of these incipient reduction processes;[30,31] these methods are used here in order to extract initial H_2 reduction rates. These rates are reported in Figure 8b as a function of MoO_x surface density for samples treated at 873 K, for $21MoO_x/ZrO_2$ treated at 723 and 773 K, and for $11MoO_x/ZrO_2$ treated at 773 K (3.5 Mo/nm^2). In samples with low surface densities (0.5−6.4 Mo/nm^2) and containing predominately MoO_x monomers and oligomers, initial H_2 reduction rates increased markedly with increasing surface density (Figure 8b), except for $11MoO_x/ZrO_2$ treated at 873 K (4.5 Mo/nm^2), which showed a higher reduction rate than all other MoO_x-containing samples. The $ZrMo_2O_8$-containing sample (8.4 Mo/nm^2, treated at 873 K) showed a higher reduction rate than those containing predominately oligomeric MoO_x structures (Figure 8b).

SCHEME 1: Reaction Network for Dimethyl Ether Reactions on MoO_x-Based Catalysts

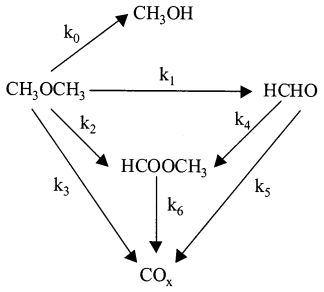

4. Discussion

The nonzero primary selectivities for CH_3OH, HCHO, MF, DMM, and CO_x (Figures 1 and 2) show that these products can be formed directly from dimethyl ether. Primary HCHO products react in secondary reactions that lead to a decrease in HCHO selectivity with increasing residence time. The concurrent increase in methylformate and CO_x selectivities implicate these species as products of secondary HCHO reactions. The small effects of residence time on CH_3OH selectivities indicate that CH_3OH is less reactive than HCHO or DME on these catalysts. DME hydration reactions do not appear to be responsible for the formation of CH_3OH, because CH_3OH formation rates are unaffected by the increase in H_2O concentration that accompanies an increase in DME conversion. Instead, it appears that CH_3OH forms via hydrogen transfer between CH_3O* adsorbed species, with the ultimate formation of one CH_3OH and one HCHO molecule.[32] Similar selectivity trends were observed on samples containing MoO_x and $ZrMo_2O_8$, suggesting that primary and secondary reaction pathways are similar on $ZrMo_2O_8$ and MoO_x domains.

The observed effects of residence time on selectivity are consistent with the reaction pathways shown in Scheme 1. These pathways include primary DME reactions to form CH_3OH, HCHO, MF, and CO_x, and reactions of HCHO (to MF and CO_x) and of MF (to CO_x). DMM formation from DME is not included in the kinetic analysis, because of the low DMM selectivities observed (<1%). The weak effects of residence time on CH_3OH selectivity led us to neglect secondary reactions of CH_3OH in our kinetic analysis.

At low DME and O_2 conversions, DME and O_2 concentrations are essentially independent of residence time and at the low H_2O concentrations prevalent at these DME conversions,

the inhibiting effects of water on reaction rates (Figure 5) can be neglected. For the DME (80 kPa) and O_2 (18 kPa) pressures of this study, reaction rates for each primary DME reaction in Scheme 1 can then be assumed to be pseudo zero-order in DME and O_2 (Figures 3 and 4b) and given by

$$r_0 = k_0 \tag{1}$$

$$r_1 = k_1 \tag{2}$$

$$r_2 = k_2 \tag{3}$$

$$r_3 = k_3 \tag{4}$$

where r_i is the rate of reaction i per Mo atom and k_i is the pseudo zero-order rate constant for reaction i.

The kinetics for secondary HCHO reactions to form MF and CO_x (Scheme 1) are likely to show a complex dependence on DME partial pressure. The nearly constant DME partial pressure along the catalyst bed allows the rates of these secondary reactions to be expressed only as a function of the concentration of the primary product involved in a given secondary reaction, which increases as DME conversion increases along the catalyst bed:

$$r_4 = k_4 C_B \tag{5}$$

$$r_5 = k_5 C_B \tag{6}$$

In these equations, r_j is the rate of reaction j per Mo atom and k_j is the pseudo first-order rate constant for reaction j, and C_B is the HCHO concentration. The dependence of HCHO selectivity (CH_3OH-free basis) (S_B) at relatively low DME conversions is then given by

$$S_B = S_B^\circ\left[1 - \frac{1}{2}(k_4 + k_5)C_{Ao}\cdot\upsilon\right]$$

$$S_B^\circ = k_1/(k_1 + k_2 + k_3) \tag{7}$$

in which S_B° is the primary HCHO selectivity, C_{Ao} is the inlet DME concentration, and υ is the g-atom Mo/inlet molar DME rate (g-atom Mo-s/mol DME) (see details in Appendix). The values of k_1, k_2, and k_3 can be estimated from the primary rates for HCHO, MF, and CO_x formation (CH_3OH-free). The value of $[(k_4 + k_5)C_{Ao}]$ can be obtained from the dependence of S_B on υ given by eq 7.

HCHO selectivities and yields depend on the relative rates of primary reactions that form HCHO, MF, and CO_x and of secondary HCHO reactions that also form MF and CO_x (Scheme 1). The $k_1/(k_2 + k_3)$ ratio provides a measure of the primary selectivity to HCHO, while the $k_1/(k_4 + k_5)$ ratio reflects the relative rates of primary HCHO formation and of secondary HCHO reactions to form MF and CO_x. The $k_1/(k_4 + k_5)$ ratio can be reflected by the $k_1/((k_4 + k_5)C_{Ao})$ ratio for a given inlet DME concentration, C_{Ao}. Higher values of $k_1/(k_2 + k_3)$ and of $k_1/((k_4 + k_5)C_{Ao})$ lead to higher HCHO selectivities at all DME conversion levels. Taken together, these two kinetic parameters determine the maximum attainable HCHO yields in DME oxidation reactions.

Figures 9a and 9b show the effects of MoO_x surface density on $k_1/(k_2 + k_3)$ and $k_1/((k_4 + k_5)C_{Ao})$ values, respectively. As MoO_x surface density increases in MoO_x-containing samples, $k_1/(k_2 + k_3)$ values initially increased and then reached a constant value (~8) at surface densities above 10 Mo/nm^2. On $ZrMo_2O_8$-containing samples, $k_1/(k_2 + k_3)$ values were ~4 and they were

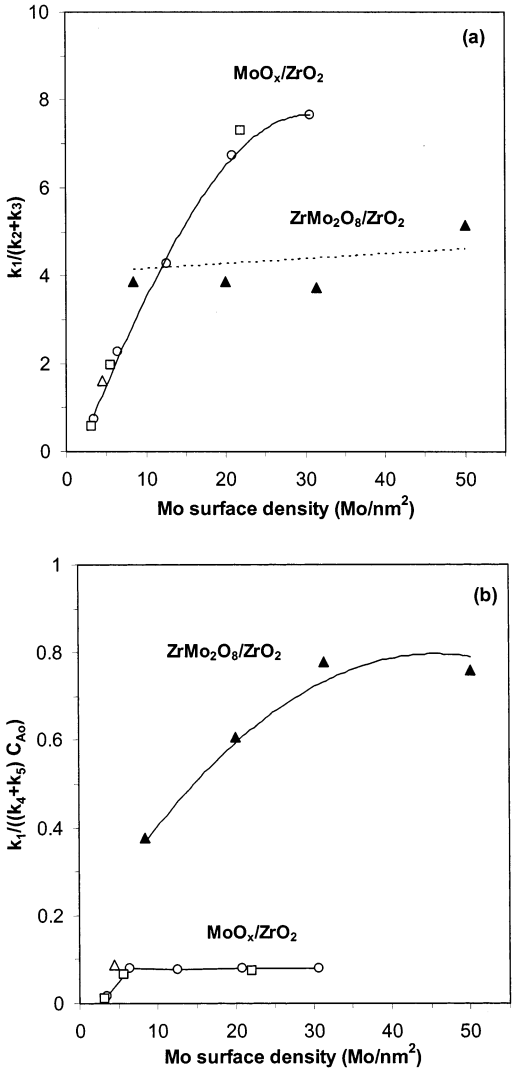

Figure 9. Dependence of $k_1/(k_2 + k_3)$ ratios (a) and $k_1/((k_4 + k_5)C_{Ao})$ ratios (b) (C_{Ao}: inlet CH_3OCH_3 concentration) on MoO_x surface density for MoO_x/ZrO_2 catalysts (pretreated in air at 723 K (□), 773 K (○), and 873 K (△, ▲)) (513 K, 80 kPa CH_3OCH_3, 18 kPa O_2, 2 kPa N_2).

unaffected by MoO_x surface density (8.4−50.1 Mo/nm^2). These trends in rate constant ratios parallel those discussed earlier for primary HCHO selectivities on MoO_x/ZrO_2 as a function of MoO_x surface density for samples with the two predominant types of MoO_x species (Figure 7a).

Values of $k_1/((k_4 + k_5)C_{Ao})$ ratios increased to constant values of ~0.09 and ~0.80 as the MoO_x surface density increased on MoO_x and $ZrMo_2O_8$ samples at the constant C_{Ao}, respectively (Figure 9b). Thus, it appears that exposed ZrO_2 surfaces favor secondary HCHO reactions to form MF and CO_x; these secondary reactions do not appear to reflect the presence of Mo−O−Zr structures, which become less abundant as MoO_x domains grow with increasing MoO_x surface density, because $ZrMo_2O_8$ surfaces actually show much lower secondary reaction rates. The $k_1/((k_4 + k_5)C_{Ao})$ ratios on $ZrMo_2O_8$ domains are much larger than on MoO_x domains and they lead to the weaker effects of residence time on HCHO selectivity observed on $ZrMo_2O_8$ surfaces compared with MoO_x surfaces (Figures 1 and 2). These effects of MoO_x surface density and MoO_x domain structure differ somewhat from those reported for propane oxidative dehydrogenation (ODH) on MoO_x/ZrO_2.[28] In that case, $ZrMo_2O_8$ domains led to higher ODH areal rates and to higher CO_x selectivities in both primary and secondary oxidation

reactions. Also, first-order rate constants for propene combustion (k_3') were much higher than for propane dehydrogenation (k_1') ($k_1'/k_3' \sim 0.03$)[28] on $ZrMo_2O_8$, while primary HCHO synthesis rate constants (k_1) are similar to those for secondary HCHO reactions ($k_4 + k_5$) on $ZrMo_2O_8$. This reflects, at least in part, the relative energies of the bonds involved in DME and alkane primary and secondary reactions. While the allylic C−H bonds in propene (361 kJ/mol) are much weaker than the secondary C−H bonds in propane (401 kJ/mol), the difference in the dissociation energy for C−H bonds in DME (389 kJ/mol) and HCHO (365 kJ/mol) are smaller than between propane and propene (24 vs 40 kJ/mol). Also, while propene is expected to bind more strongly than propane on Lewis acid sites (Mo^{6+}) because its π-bond makes it more basic than propane, the lone-pair electrons of oxygen in DME lead to its stronger adsorption on acid sites relative to HCHO.[14,36,37] Taken together, the molecular properties of reactants and products in these two reactions appear to account for the higher attainable yields for oxidative reactions of DME compared with similar reactions of propane.

In contrast with the strong dependence of $k_1/(k_2 + k_3)$ and $k_1/((k_4 + k_5)C_{Ao})$ values on MoO_x surface density, these two kinetic parameters did not change significantly with changes in the partial pressures of DME, O_2, and H_2O. These changes in $k_1/(k_2 + k_3)$ values led to the small parallel effects on primary HCHO selectivity observed with changes in DME, O_2, and H_2O pressures shown in Figures 3−5. The $k_1/((k_4 + k_5)C_{Ao})$ values increased from 0.26 to 0.31 and from 0.28 to 0.34 with increasing the DME and H_2O partial pressures in the range 10−80 kPa and 0−15 kPa, respectively; the $k_1/((k_4 + k_5)C_{Ao})$ values remained almost constant (∼0.27) as the O_2 partial pressure changed from 5 to 40 kPa. This indicates that HCHO selectivities and maximum attainable yields at a given DME conversion level depend only slightly on the partial pressures of DME, O_2, and H_2O.

The activity of surface sites on MoO_x domains for DME oxidation to HCHO depends sensitively on the structural evolution induced by an increase in the MoO_x surface density (Figure 6a,b). The predominant presence of MoO_x monomers and two-dimensional oligomers in MoO_x/ZrO_2 samples with surface densities below 6.4 Mo/nm^2 exposes most MoO_x species at surfaces, where these species are accessible to reactants. As a result, the measured DME reaction rates (per Mo atom) represent turnover rates (per exposed MoO_x). These turnover rates increase with increasing MoO_x surface density (0.5−6.4 Mo/nm^2) (Figure 6a), indicating that the reactivity of MoO_x surfaces increases as the size and dimensionality of MoO_x domains increases. These higher turnover rates parallel the higher initial H_2 reduction rates (per Mo atom) measured for larger domains (Figure 8b). The more facile reduction of larger domains, and the consequently faster catalytic redox cycles, reflect more effective delocalization of the negative charge by these larger domains. These electronic effects also lead to lower absorption edge energies in the UV−visible spectrum of larger domains, as a result of the effectiveness of larger domains in delocalizing the electrons transferred from the oxygen atoms to the metal centers in the electronic transition responsible for the absorption edge in the UV−visible spectrum.[33]

DME reaction rates (per Mo) decreased with increasing surface density in more densely packed surfaces (>6.4 Mo/nm^2) (Figure 6a), in which polymolybdate and three-dimensional MoO_3 crystallites become the predominant structures. DME reaction rates decreased with increasing nominal MoO_x surface density on $ZrMo_2O_8$ throughout the entire surface density range

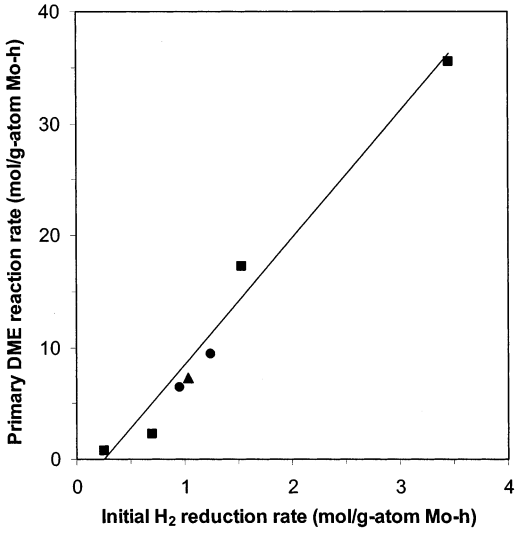

Figure 10. Dependence of primary DME reaction rate at 513 K on initial H_2 reduction rate at 623 K for MoO_x/ZrO_2 catalysts treated in air at 723 K (▲), 773 K (●), and 873 K (■).

(8.4−50.1 Mo/nm^2) (Figure 6a). On both MoO_x and $ZrMo_2O_8$ structures, this reflects the nucleation of three-dimensional clusters, which render an increasing fraction of the MoO_x species inaccessible to reactants by placing them within crystallites. The surface density required for maximum rates (per Mo) on MoO_x-containing samples (6.4 Mo/nm^2) is slightly higher than the theoretical polymolybdate monolayer value (∼5.0 Mo/nm^2).[38] This reflects a compromise between the lower accessibility and the higher reactivity of MoO_x surfaces as the size and dimensionality of MoO_x domains increase.

MoO_x surface density effects on areal DME reaction rates (Figure 6b) confirmed these conclusions. Areal rates and primary HCHO selectivities both reached constant values at Mo surface densities of ∼10 Mo/nm^2 on both MoO_x (0.08 mmol/m^2-h; 90%) and $ZrMo_2O_8$ (0.45 mmol/m^2-h; 80%), but the rates are significantly higher on $ZrMo_2O_8$ surfaces. These constant values indicate that all exposed surfaces contain predominately MoO_3 and $ZrMo_2O_8$ species with active surface structures, the kinetic behavior of which is unaffected by further increases in size or dimensionality. This could reflect a similar surface reactivity for two-dimensional and three-dimensional MoO_x structures, or merely the predominant contribution from polymolybdate monolayers on ZrO_2 or surface layers of $ZrMo_2O_8$ to the exposed surfaces , without significant contributions from any large MoO_3 crystallites also present. The higher areal rates measured on $ZrMo_2O_8$ samples are consistent with their more reducible nature, as shown by the rate of their stoichiometric reduction in H_2 (Figure 8b). The more reducible nature of $ZrMo_2O_8$ appears to reflect a structure consisting of two-dimensional networks of alternating MoO_4 tetrahedra and ZrO_6 octahedra (corner-shared), which differs markedly from the layers of corner-sharing MoO_6 octahedra in MoO_3 crystallites. The atomic connectivity between Mo^{6+} and the less electronegative Zr^{4+} cations in $ZrMo_2O_8$ may favor the electron transfer and the activation of Mo−O bonds during the reduction in H_2 and the DME reaction.

Figure 10 shows the observed parallel increase in primary DME reaction rates (per Mo atom, at 513 K) and initial reduction rates in H_2 (per Mo atom, at 623 K) with increasing MoO_x surface density. These data correspond to samples in which most Mo species are exposed at surfaces, because only then catalytic reaction rates and reduction rates reflect their respective surface reaction rates. These data clearly show that

the effects of domain size and the differences between MoO_x and $ZrMo_2O_8$ surfaces in HCHO synthesis from DME arise from the varying ability of such species to reduce as part of the kinetically relevant C−H bond activation steps within catalytic cycles. Similar trends were observed for DME reactions on MoO_x species on other supports[27] and on dispersed VO_x domains.[39] These correlations between the reducibility of the active oxides and their activity parallel similar effects reported for other oxidation reactions involving MoO_x and VO_x lattice oxygen atoms and Mars-van Krevelen redox cycles, such as the oxidative dehydrogenation reactions of alkanes[30,31,33,40] and alcohols.[15,41−43]

5. Conclusions

Dimethyl ether conversion to formaldehyde occurs with high selectivity at ~500 K on MoO_x−ZrO_2. Reaction rates are significantly higher than those reported previously in the patent literature. The catalysts used consist of MoO_x oligomers and $ZrMo_2O_8$. Dimethyl ether reaction rates (per Mo atom) increase markedly with increasing MoO_x surface density in the 2.2 to 6.4 Mo/nm^2 range as two-dimensional polymolybdate domains grow and ultimately form MoO_3 clusters. The rates of reduction of these materials in H_2 increase in parallel with increasing MoO_x surface density, suggesting that redox cycles and kinetically relevant reduction steps are involved in dimethyl ether reactions and that the rate of such steps increases with increasing reducibility of MoO_x domains. Reaction rates are nearly zero-order in O_2, while the dependence on dimethyl ether decreases from first-order at low pressures (<40 kPa) to zero-order at higher pressures (>60 kPa). These kinetic dependences are consistent with this proposal. Above 6.4 Mo/nm^2, reaction rates decrease with increasing surface density because MoO_3 and $ZrMo_2O_8$ (after treatment in air at 723−773 and 873 K, respectively) with increasingly inaccessible MoO_x species form. Reaction rates (per BET surface area) approach constant values as exposed surfaces become entirely covered with active MoO_x or $ZrMo_2O_8$. The latter are more reducible in H_2 than MoO_x surfaces and show higher areal HCHO synthesis rates. DME reacts directly to form HCHO, methyl formate, and CO_x, with pseudo zero-order rate constants k_1, k_2, and k_3. Methylformate (k_4) and CO_x (k_5) also form in secondary reactions of HCHO. The primary formaldehyde selectivity (and the relevant kinetic ratio, $k_1/(k_2 + k_3)$) increases with increasing MoO_x surface density on MoO_x-containing samples and reaches values of 80−90% above 10 Mo/nm^2. The kinetic ratio describing the extent of secondary reactions ($k_1/((k_4 + k_5)C_{Ao})$) also increases with increasing MoO_x surface density to values of ~0.1 and 0.8 on MoO_x and $ZrMo_2O_8$ structures (at the constant inlet DME concentration C_{Ao}, respectively. It appears that more selective active sites form as ZrO_2 surfaces become increasingly covered with MoO_x or $ZrMo_2O_8$ structures, which leads to more selective structures for the synthesis of HCHO from dimethyl ether.

Acknowledgment. This study was supported by BP as part of the Methane Conversion Cooperative Research Program at the University of California at Berkeley. The authors acknowledge helpful technical discussions with Drs. Theo Fleisch and John Collins of BP. The authors also thank Dr. Kaidong Chen for the synthesis of some of the supported MoO_x samples.

Appendix

The conversion of DME (A) in a plug-flow reactor for the reaction scheme in eqs 1−4 is given at relatively low conversions (or at any conversion in the zero-order reaction regime) by

$$\frac{dX_A}{d\varsigma} = \upsilon\cdot(k_1 + k_2 + k_3) \tag{A1}$$

where

X_A = fractional DME conversion (on a DME-free basis)

υ = g-atom Mo/inlet molar DME rate (g-atom Mo-s/mol DME)

k_i = rate constants for primary DME reactions (mol DME/g-atom Mo-s)

ς = fractional distance along the reactor

The solution to this equation is

$$X_A = (k_1 + k_2 + k_3)\cdot\upsilon \tag{A2}$$

The HCHO concentration (C_B) and molar rates (F_B) are given by

$$\frac{1}{\upsilon}\frac{d(F_B/F_{Ao})}{d\varsigma} = 2k_1 - (k_4 + k_5)C_B \tag{A3}$$

where F_{Ao} is the inlet molar DME rate and the rate constants are those for eqs 5 and 6 in the text. At relatively low DME conversions, changes in the total number of moles can be neglected and eq A3 becomes

$$\frac{1}{\upsilon C_{Ao}}\frac{dC_B}{d\varsigma} = 2k_1 - (k_4 + k_s)C_B \tag{A4}$$

in which C_{Ao} is the inlet DME concentration and the inlet HCHO concentration is assumed to be zero. The solution to this equation is

$$C_B = \frac{2k_1}{(k_4 + k_5)}[1 - \exp\{-(k_4 + k_5)C_{Ao}\upsilon\}] \tag{A5}$$

The HCHO selectivity (S_B) (CH_3OH-free basis) is then given by

$$S_B = \frac{C_B}{2C_{Ao}X_A} = \frac{k_1}{(k_1 + k_2 + k_3)}\cdot\frac{1}{(k_4 + k_5)\upsilon C_{Ao}}\cdot [1 - \exp\{-(k_4 + k_5)C_{Ao}\upsilon\}] \tag{A6}$$

When the observed selectivity changes as a result of changes in υ are small, a series expansion of the exponential to second-order term two gives

$$S_B = S_B^{\circ}\left[1 - \frac{1}{2}(k_4 + k_5)C_{Ao}\cdot\upsilon\right] \tag{A7}$$

where the primary HCHO selectivity S_{B° (CH_3OH-free basis) is

$$S_B^{\circ} = \frac{k_1}{k_1 + k_2 + k_3}$$

The primary selectivity is obtained from the *y*-intercept of a HCHO selectivity vs υ plot; the slope of the plot is $-(1/2)(k_4$

$+ k_5)C_{Ao}$, from which the reported values of $[k_1/(k_4 + k_5)C_{Ao}]$ are readily obtained.

References and Notes

(1) Lunsford, J. H.; Ito, T. *Nature* **1985**, *314*, 721.
(2) Pitchai, R.; Klier, K. *Catal. Rev.−Sci. Eng.* **1986**, *28*, 13.
(3) Lee, J. S.; Oyama, S. T. *Catal. Rev.−Sci. Eng.* **1988**, *30*, 249.
(4) Tabata, K.; Teng Y.; Takemoto, T.; Suzuki, E.; Banares, M. A.; Pena, M. A.; Fierro, J. L. G. *Catal. Rev.−Sci. Eng.* **2002**, *44*, 1.
(5) Otsuka, K.; Wang, Y. *Appl. Catal.* **2001**, *222*, 145.
(6) Cooper, C. A.; Hammond, C. R.; Hutchings, G. J.; Taylor, S. H.; Willock, D. J.; Tabata, K. *Catal. Today* **2001**, *71*, 3.
(7) Faraldos, M.; Banares, M. A.; Anderson, J. A.; Hu, H.; Wachs, I. E.; Fierro, J. L. G. *J. Catal.* **1996**, *160*, 214.
(8) Bafas, I. C.; Constantinou, I. E.; Vayenas, C. G. *Chem. Eng. J.* **2001**, *82*, 109.
(9) Barbero, J. A.; Banares, M. A.; Pena, M. A.; Fierro, J. L. G. *Catal. Today* **2001**, *71*, 11.
(10) Berndt, H.; Martin, A.; Bruckner, A.; Schreier E.; Muller, D.; Kosslick, H.; Wolf, G. U.; Lucke, B. *J. Catal.* **2000**, *191*, 384.
(11) Tomomi, S.; Kido, A.; Azuma, N.; Ueno, A.; Udagawa, Y. *J. Catal.* **2000**, *190*, 118.
(12) Amir-Ebrahimi, V.; Rooney, J. J. *J. Mol. Catal.* **1989**, *50*, L17.
(13) Lefferts, L.; van Ommen, J. G.; Ross, J. R. H. *Appl. Catal.* **1986**, *23*, 385.
(14) Tatibouet, J. M. *Appl. Catal. A: General* **1997**, *148*, 213.
(15) Deo, G.; Wachs, I. E. *J. Catal.* **1994**, *146*, 323.
(16) Hara, M.; Kawamura, M.; Kondo, J. N.; Domen, K.; Maruya, K. *J. Phys. Chem.* **1996**, *100*, 14462.
(17) Ouyang, F.; Yao, S. *J. Phys. Chem.* **2000**, *104*, 11253.
(18) Tadenuma, H.; Murakami, T.; Mitsushima, H. U.S. Patent 3,655,771, 1972.
(19) Lewis, R. M.; Ryan, R. C.; Slaugh, L. H. U.S. Patent 4,442,307, 1984.
(20) Lewis, R. M.; Ryan, R. C.; Slaugh, L. H. U.S. Patent 4,439,624, 1984.
(21) Lewis, R. M.; Ryan, R. C.; Slaugh, L. H. U.S. Patent 4,435,602, 1984.
(22) Hagen, G. P.; Spangler, M. J. U.S. Patent 6,265,528, 2001.
(23) Li, J.-L.; Zhang, X.-G.; Inui, T. *Appl. Catal. A: General* **1996**, *147*, 23.
(24) Fleisch, T. H.; Basu, A.; Gradassi, M. J.; Masin, J. G. *Stud. Surf. Sci. Catal.* **1997**, *107*, 117.
(25) Shikada, T.; Ohno, Y.; Ogawa, T.; Ono, M.; Mizuguchi, M.; Tomura, K.; Fujimoto, K. *Stud. Surf. Sci. Catal.* **1998**, *119*, 515.
(26) Liu, H.; Iglesia, E. *J. Catal.* **2002**, *208*, 1.
(27) Liu, H.; Cheung, P.; Iglesia, E. *J. Catal.*, in press.
(28) Chen, K.; Xie, S.; Iglesia, E.; Bell, A. T. *J. Catal.* **2000**, *189*, 421.
(29) Xie, S.; Chen, K.; Bell, A. T.; Iglesia, E. *J. Phys. Chem.* **2000**, *104*, 10059.
(30) Chen, K.; Xie, S.; Bell, A. T.; Iglesia, E. *J. Catal.* **2000**, *195*, 244.
(31) Chen, K.; Xie, S.; Bell, A. T.; Iglesia, E. *J. Catal.* **2001**, *198*, 232.
(32) Liu, H.; Cheung, P.; Iglesia, E. Unpublished results.
(33) Chen, K.; Bell, A. T.; Iglesia, E. *J. Catal.* **2002**, *209*, 35.
(34) Arnoldy, P.; de Jonge, J. C. M.; Moulijn, J. A. *J. Phys. Chem.* **1985**, *89*, 451.
(35) Regalbuto, J. R.; Ha, J. W. *Catal. Lett.* **1994**, *29*, 189.
(36) Chen, K.; Bell, A. T.; Iglesia, E. *J. Phys. Chem.* **2000**, *104*, 1292.
(37) Albonetti, S.; Cavani, F.; Trifiro, F. *Catal. Rev.−Sci. Eng.* **1996**, *38*, 413.
(38) Xie, Y. C.; Tang, Y. Q. *Adv. Catal.* **1990**, *37*, 1.
(39) Cheung, P.; Liu, H.; Iglesia, E. Unpublished results.
(40) Abello, M. C.; Gomez, M. F.; Cadus, L. E. *Catal. Lett.* **1998**, *83*, 185.
(41) Kim, D. S.; Wachs, I. E.; Segawa, K. *J. Catal.* **1994**, *146*, 268.
(42) Zhang, W.; Desikan, A.; Oyama, S. T. *J. Phys. Chem.* **1995**, *99*, 14468.
(43) Niwa, M.; Sano, M.; Yamada, H.; Murakami, Y. *J. Catal.* **1995**, *151*, 285.